Long-time evolution of a drop size distribution by coalescence in a linear flow

A. E. Ismail* and M. Loewenberg
Department of Chemical Engineering, Yale University, New Haven, Connecticut 06520-8286, USA
(Received 22 April 2003; revised manuscript received 5 December 2003; published 30 April 2004)

The growth of spherical drops by coalescence in simple shear and axisymmetric straining flows has been numerically investigated, and the long-time scaling behavior of the system was explored. It is shown that hydrodynamic interactions qualitatively modify the the collision kernel in the population balance equation and thus alter the evolution of the drop size distribution at long times. In the presence of hydrodynamic interactions, the number of drops in the system decays as t^{-1}, and the average drop size grows as $e^{\sqrt{t}}$; in the absence of hydrodynamic interactions, these quantities evolve exponentially at long times. Hydrodynamic interactions lead to broader drop size distributions, and cause the influence of initial conditions to decay with time. Drops undergoing thermocapillary migration are shown to exhibit similar features. Our results are shown to be consistent with the established theory for the scaling behavior of aggregating systems. It is shown that the theory applies even in certain cases where the binary collision kernel does not have the assumed form. In the presence of hydrodynamic interactions, the scaling regime is attained slowly (logarithmically).

DOI: 10.1103/PhysRevE.69.046307 PACS number(s): 47.55.Kf, 82.70.Kj

I. INTRODUCTION

The growth of particle clusters by coagulation in a dispersion is important for a wide range of natural and industrial processes, such as the growth of rain drops [1], blending of immiscible polymers [2], production of ceramic particles [3], and the flocculation of suspended colloidal particles in food processing [4] and water treatment [5]. The cluster-size distribution evolves in time according to the Smoluchowski equation [6,7]

$$\frac{\partial n_k}{\partial t} = \frac{1}{2} \sum_{i+j=k} K(v_i, v_j) n_i n_j - n_k \sum_{j=1}^{\infty} K(v_k, v_j) n_j, \tag{1.1}$$

where n_k is the number density of clusters with volume v_k and the kernel function $K(u,v)$ represents the rate of coagulation of clusters with volumes u and v. The order-p moment of the cluster-size distribution is defined as

$$M_p = \sum_{k=1}^{\infty} v_k^p n_k. \tag{1.2}$$

For homogeneous kernel functions, Eq. (1.1) is invariant under a group of similarity transformations for which there exist scaling solutions for large cluster sizes [8–10]. The scaling behavior of Eq. (1.1) depends on the degree of homogeneity m of the kernel function

$$K(bu, bv) = b^m K(u,v), \tag{1.3}$$

where b is a constant. For $m>1$, the average cluster size s diverges at a finite (gelation) time; otherwise, s increases monotonically. For $m \leqslant 1$, the large-cluster scaling regime corresponds to the long-time behavior of the system.

The scaling behavior for systems with homogeneous kernel functions also depends qualitatively on the exponent μ, defined by

$$K(u, \kappa u) \sim u^m \kappa^{\mu}, \quad \kappa \to 0, \tag{1.4}$$

where κ is the size ratio of clusters. Kernel functions are classified according to whether $\mu>0$ (class I), $\mu=0$ (class II), or $\mu<0$ (class III) [8]. For class I kernels, collisions between the largest clusters in the system dominate the growth of the cluster size distribution, whereas collisions between small and large clusters controls the evolution for class III systems. Class II kernel functions are the intermediate case where collisions between large clusters and collisions between disparate size clusters are both important.

The theory for systems described by Eq. (1.1) is considerably less developed for kernel functions that do not satisfy the functional form (1.3) and (1.4). Thus, many problems can only be studied by numerical simulation [11–18]. To date, however, there has been little overlap between numerical and theoretical studies: the scaling regime has rarely been explored by numerical simulation. Thus, little is known about the extent to which theoretical results for the asymptotic scaling regime apply either for finite times and away from gelation or for kernel functions that do not have the assumed functional form (1.3) and (1.4).

Previous studies have often relied on drastically simplified models for the kernel function due to the difficulty of describing the complex aggregation processes and cluster geometries relevant to most problems [3,19]. An exception is liquid-liquid suspensions (emulsions) under strong surface tension conditions where drop deformation is negligible so that ''clusters'' are spherical. Moreover, pair interactions and ''aggregation'' (i.e., coalescence) can be modeled for spherical drops in Stokes flow with only modest computational effort [16–18,20,21]. Emulsions of spherical drops thus provide an attractive model system suitable for comparison with experiments [9–11,22].

*Present address: Department of Chemical Engineering, Massachusetts Institute of Technology, Cambridge, MA 02139.

 ©2004 The American Physical Society

For these reasons, we restrict the present study to emulsions of spherical drops in Stokes flow. Specifically, we consider the growth of spherical drops by coalescence in linear flows. This choice is motivated by the theoretical prediction that hydrodynamic interactions qualitatively affect the long-time evolution of this system. The growth of drops undergoing thermocapillary migration is also considered. Our results show the extent to which the asymptotic long-time theory describes the behavior of the system at finite times. Moreover, we provide examples where the long-time scaling theory applies even though the kernel function does not obey the form (1.3) and (1.4).

The numerical model is described in Sec. II, and the relevant theory is reviewed in Sec. III. Numerical results are compared to theoretical predictions in Sec. IV. Results for thermocapillary migration are discussed in Sec. V. Concluding remarks follow in Sec. VI.

II. KERNEL FUNCTION

The collision kernel has the form

$$K(u,v)=K_0(u,v)E, \tag{2.1}$$

where K_0 is the collision kernel for noninteracting drops. Pairwise hydrodynamic interactions are incorporated through the collision efficiency E [20,23], as described in the Appendix. For neutrally-buoyant non-Brownian drops in a linear flow,

$$K_0(u,v)=C\dot{\gamma}(u^{1/3}+v^{1/3})^3, \tag{2.2}$$

where $\dot{\gamma}$ is the strain rate, and C is a flow-dependent constant. According to Eq. (1.3), K_0 is a homogeneous kernel with degree $m=1$. We consider below simple shear flow represented in Cartesian coordinates (x,y,z) by

$$\mathbf{u}=\dot{\gamma}(y,0,0), \tag{2.3}$$

and axisymmetric straining flow

$$\mathbf{u}=\dot{\gamma}(-\tfrac{1}{2}r,0,z), \tag{2.4}$$

where $r=\sqrt{x^2+y^2}$ is the distance from the symmetry axis. For shear flow, $C=\pi^{-1}$; for axisymmetric strain, $C=(8/3)^{1/2}$. Henceforth, time is nondimensionalized by $(C\dot{\gamma}M_1)^{-1}$, where M_1 is the conserved volume fraction of the drop phase, and drop volumes are nondimensionalized by the volume of the smallest drop in the system.

We consider a dilute suspension of spherical drops with viscosity $\lambda\eta$ in a fluid with viscosity η, and we introduce the viscosity parameter $\Lambda=1/(1+\lambda)$. Stokes flow conditions apply. The effects of surfactants and nonhydrodynamic forces such as van der Waals attraction are neglected. Under these assumptions, E depends on the parameters κ and Λ and on the flow type but not on the drop size [20]. According to the discussion in Sec. I, it follows that hydrodynamic interactions may affect the class but not the degree of the kernel function. Thus K is a first-degree kernel.

In the absence of particle interactions $(E=1)$, the collision kernel is a class II $(\mu=0)$ first-degree homogeneous function. In this case, the evolution of the system in dimensionless variables is independent of flow-type and viscosity ratio.

Hydrodynamic interactions hinder coalescence, particularly for extreme size ratios because smaller drops tend to be convected around, rather than captured by, larger drops. Thus, the system evolves more slowly, and broader drop size distributions are obtained in the presence of hydrodynamic interactions. As shown in the Appendix, collision efficiencies are lower for high viscosity drops $(\Lambda\ll 1)$. This results from the fact that the near-contact lubrication resistance between drops with tangentially mobile interfaces is controlled by dissipation associated with the flow inside of the drops [24].

For $\Lambda<1$, collision efficiencies are lower in shear flow (2.3) than in axisymmetric strain (2.4). In shear flow, collision efficiencies vanish for Λ below a critical value Λ_0 given by Eq. (A12).

As shown in the Appendix, collision efficiencies in straining flow vanish in the small size-ratio-limit with exponent $\mu=1/3$, where μ is defined by Eq. (1.4). Thus, Eq. (2.1) becomes a class I kernel function in the presence of hydrodynamic interactions in straining flow. In shear flow, collision efficiencies vanish with exponent $\mu=3/2$ at a critical size ratio κ_0 but the exponent is defined by Eq. (A10). However, the numerical results presented in Sec. IV indicate that theory for class I kernel functions nonetheless describes the long-time behavior of the system.

III. SCALING BEHAVIOR

In the presence of hydrodynamic interactions (class I kernels), the evolution of the system is controlled by the coalescence of similar-size drops; in the absence of particle interactions (class II kernels), the capture of small drops by the much larger drops is also important. This picture is borne out by the analysis of Van Dongen and Ernst [8,25] for the long-time behavior of Eq. (1.1) for first-degree kernels belonging to classes I and II. Their results are summarized below.

A. Class I kernels

The scaling behavior for class I kernel functions is [25]

$$\varphi(x)=(s^2\ln s)n(v,t), \tag{3.1}$$

where $x=v/s(t)$, and $s(t)=M_2(t)/M_1$ is average drop size with moments M_p defined by Eq. (1.2). The scaling solution $\varphi(x)$ is independent of the initial conditions. The small- and large-size tails of the drop size distribution are described by [25]

$$\varphi\sim x^{-2},\ x\ll 1, \tag{3.2a}$$

$$\varphi\approx Ax^{-1}e^{-\delta x},\ x\gg 1, \tag{3.2b}$$

where

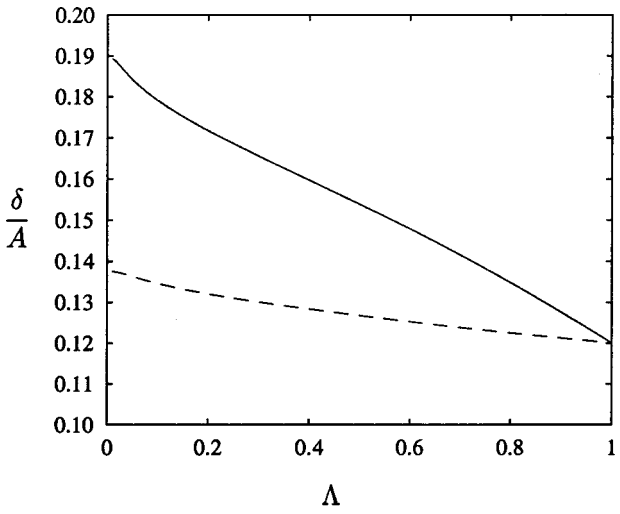

FIG. 1. Viscosity-ratio dependence of the parameter δ/A defined by Eq. (3.3) for large-size tail of scaling solution in shear flow (solid curve), and straining flow (dashed curve).

$$\frac{\delta}{A}=\frac{1}{2w_{\mathrm{I}}}\int_0^1 \frac{K(u,1-u)}{u(1-u)}du, \tag{3.3}$$

and

$$w_{\mathrm{I}}=\int_0^1 \frac{du}{u}\int_{1-u}^{\infty}\frac{dv}{v^2}K(u,v). \tag{3.4}$$

For class I kernels, the total number of drops M_0 decays algebraically

$$M_0\sim t^{-1}, \tag{3.5}$$

and the average drop size evolves as [25]

$$s\sim\exp(2\sqrt{w_{\mathrm{I}}t}). \tag{3.6}$$

Expressions (3.3) and (3.4) were evaluated for collision kernels (2.1) and (2.2) with collision efficiencies given by Eqs. (A2)–(A6). The viscosity and flow-type dependence of the parameters δ/A and w_{I} are depicted in Figs. 1 and 2. According to Eq. (3.6), the flow-type and viscosity ratio affect the average drop size at long times through the parameter w_{I}. As shown in Sec. IV B, w_{I} approximately captures the influence of flow type and viscosity ratio on the evolution of the system.

B. Class II kernels

The scaling behavior for class II kernel functions is [25]

$$\varphi(x)=s^2n(v,t), \tag{3.7}$$

where x and $s(t)$ are defined as in Eq. (3.1). For class II kernels, the scaling solution depends on the initial conditions. The small- and large-size tails of the drop size distribution are given by [25]

$$\varphi\sim x^{-2+1/w_{\mathrm{II}}},\ x\ll 1, \tag{3.8a}$$

$$\varphi\sim x^{-\beta}e^{-\alpha x},\ x\gg 1. \tag{3.8b}$$

The number of drops M_0 and the average drop size s evolve exponentially for class II kernels [25]

$$M_0\sim e^{-t}, \tag{3.9}$$

$$s\sim e^{w_{\mathrm{II}}t}. \tag{3.10}$$

The constants, $w_{\mathrm{II}}=5.62$, $\alpha=0.515$, and $\beta=1.18$ were obtained by numerical integration of Eq. (1.1), as described below.

IV. NUMERICAL SIMULATIONS

Equation (1.1) was integrated as a set of ordinary differential equations for $y_i=\log_{10}n_i$ with $i=1,2,3,\ldots,N$. Discrete drop volume spectra were obtained by considering only discrete (i.e., monodisperse, bidisperse) initial distributions. Except as noted, our numerical results correspond to monodisperse initial conditions:

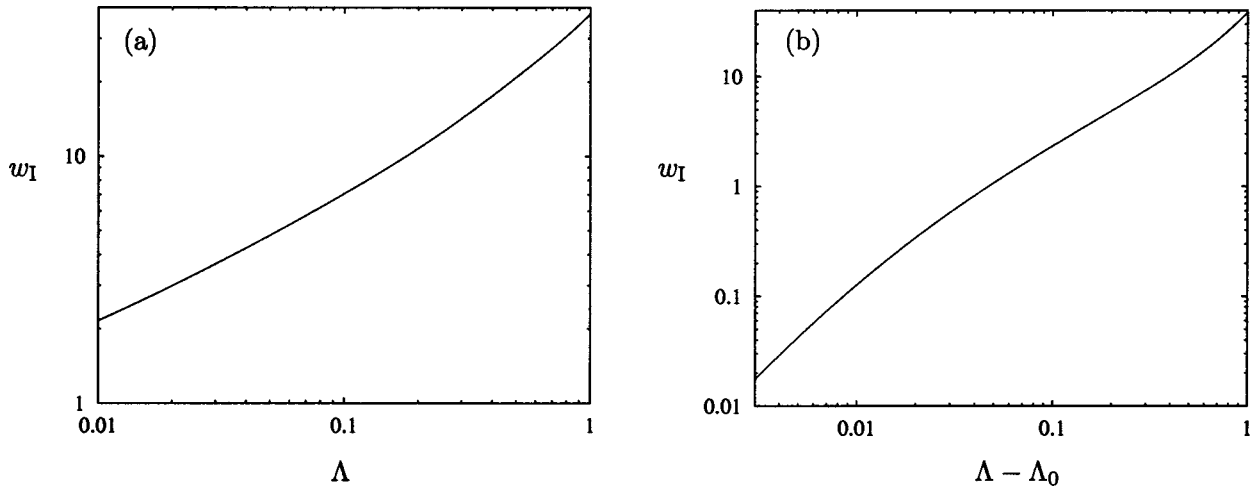

FIG. 2. Viscosity dependence of w_I defined by Eq. (3.4) for (a) straining flow, (b) shear flow [Λ_0 is the critical viscosity ratio (A12)].

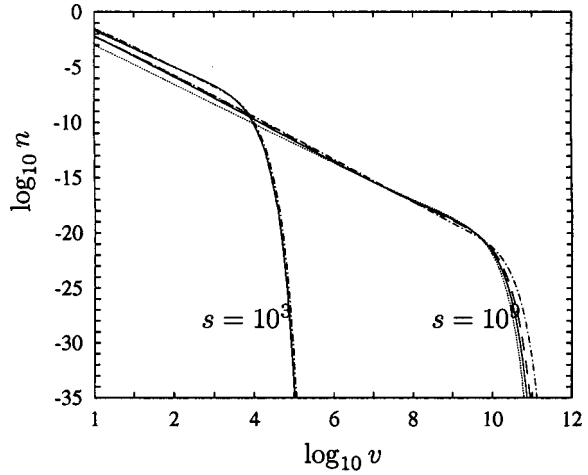

FIG. 3. Drop size distributions, average size indicated; $\Lambda = 1$ (solid curves), $\Lambda = 4\Lambda_0$ straining flow (dashed curves), $\Lambda = 4\Lambda_0$ shear flow (dot-dashed curves); noninteracting drops (dotted curves).

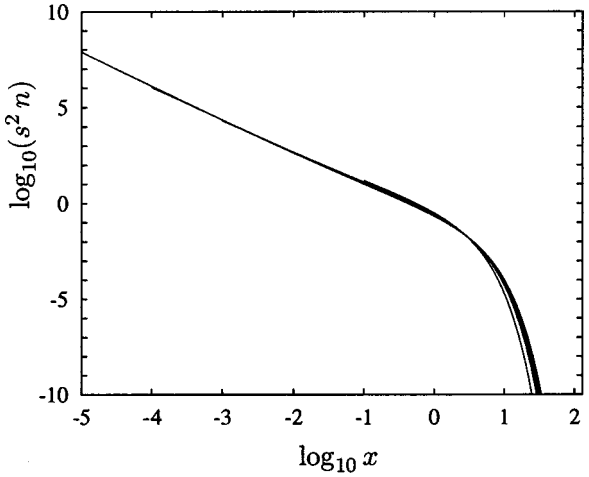

FIG. 4. Rescaled drop size distributions for noninteracting drops. In sequence from left to right, profiles correspond to $s = 10, 10^2, 10^3, 10^4, 10^8, 10^{12}, 10^{16}, 10^{20}, 10^{24}$.

$$n(v,0) = \delta(v-1). \tag{4.1}$$

A spline over a logarithmic distribution of drop volumes was used to represent the large-size tail of the distribution. The overall accuracy of the procedure is $O(1/N^4)$. In all cases, numerical convergence was achieved with $N = 800$. Collision efficiencies were calculated according to the procedure described in the Appendix.

A. Drop size distributions

Size distributions of interacting and noninteracting drops are shown in Fig. 3. The initially monodisperse drop size distributions evolve to an algebraic distribution of small drops and an exponential tail of large drops. At long times, hydrodynamic interactions increase the population of the small drops.

The approach to the scaling regime (3.7) for noninteracting drops is evident by the rescaled distributions depicted in Fig. 4. The results shown in Fig. 5 reveal that in the presence of hydrodynamic interactions, the distribution of subaverage-size drops approaches the scaling regime (3.1) more slowly, but the distribution of larger drops does not exhibit this scaling, even at extreme times (corresponding to unphysical values of s). Our results indicate that large drops exhibit a nonuniversal logarithmic evolution in the presence of hydrodynamic interactions.

For noninteracting drops, the long-time scaling for small drops (3.8a) is recovered, as shown in Fig. 6(a). Figure 6(b) reveals a logarithmic correction to the long-time scaling (3.2a) for small drops in the presence of hydrodynamic interactions. Results for a monodisperse (4.1) and a bidisperse initial drop size distribution

$$n(v,0) = \frac{1}{2}\delta(v-1) + \frac{1}{4}\delta(v-2) \tag{4.2}$$

are shown in Fig. 6 ($M_1 = 1$ for both distributions). Oscillations in the drop size distribution, resulting from bidispersed

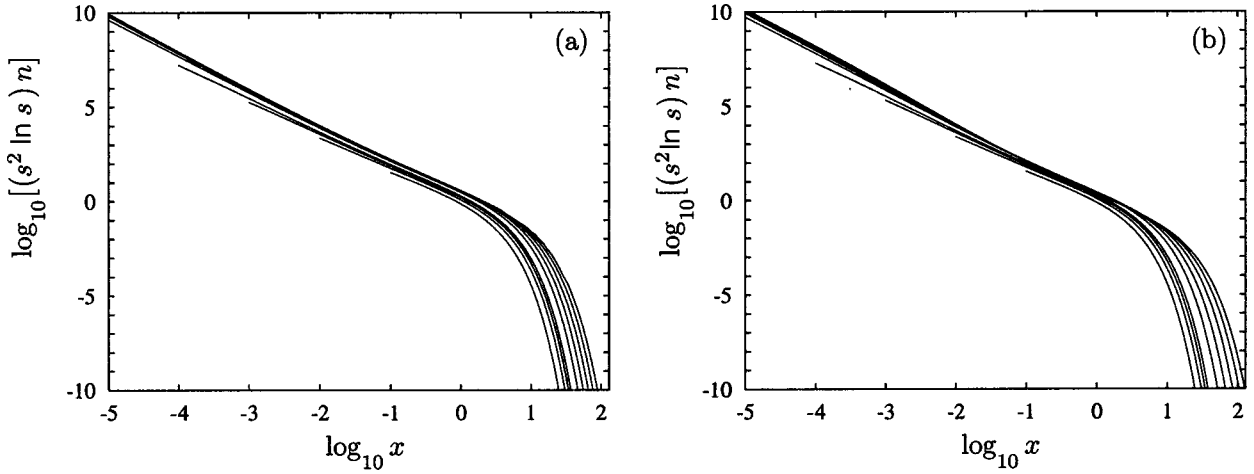

FIG. 5. Rescaled drop size distribution for hydrodynamically interacting drops, $\Lambda = 1/2$, in (a) straining flow and (b) shear flow. Profiles from left to right are the same as Fig. 4.

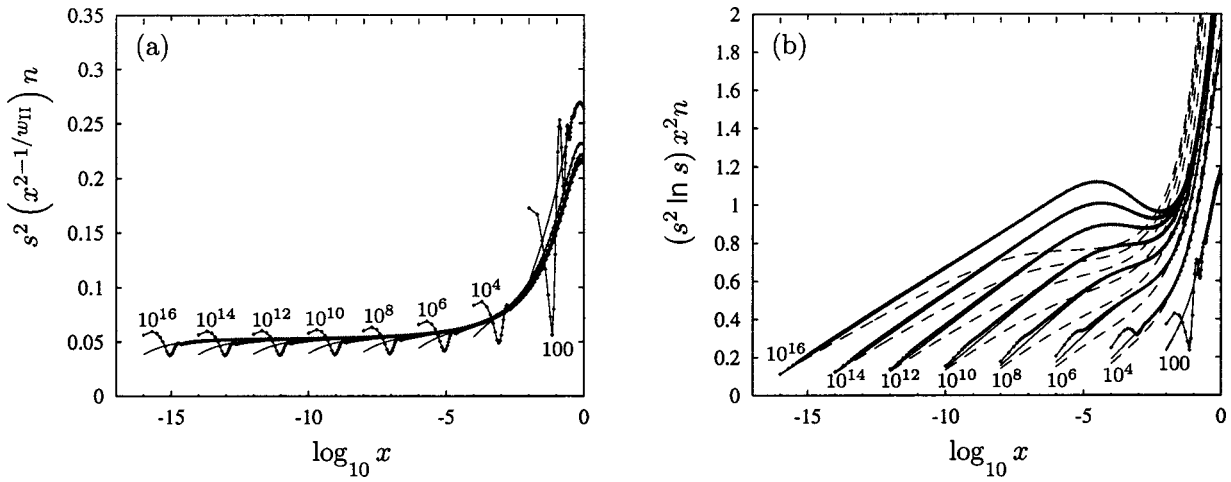

FIG. 6. Small-size tail of distribution, average size indicated; monodisperse initial conditions (4.1) (solid, dashed curves), bidisperse initial conditions (4.2) ($-\diamond-\diamond-\diamond-$); (a) noninteracting drops, (b) $\Lambda=1/2$ shear-flow (solid curves, $-\diamond-\diamond-\diamond-$), $\Lambda=1/2$ straining flow (dashed curves).

initial conditions, decay only in the presence of hydrodynamic interactions, consistent with the influence of initial conditions mentioned in Sec. III.

For noninteracting drops, the large-size tail of the drop size distribution attains the asymptotic form (3.8b) at long times, as shown in Fig. 7. Figure 8 reveals a logarithmic convergence of the parameter δ/A to the long-time result (3.3), but the individual parameters δ, A of the large size tail (3.2b) do not become stationary in the presence of hydrodynamic interactions. This is consistent with the nonuniversal behavior of large drops seen in Fig. 5.

B. Evolution of the average drop size and number of drops

The evolution of the number of drops and average drop size is depicted in Figs. 9 and 10. In the absence of hydrodynamic interactions, the system evolves exponentially at long times, as predicted by Eqs. (3.9) and (3.10). The slow approach to the long-time scaling behavior in the presence of hydrodynamic interactions (3.5) and (3.6) results from the nonuniversal evolution of the large drops discussed above. The effect of the viscosity parameter and flow type are approximately captured by rescaling time as $w_I t$.

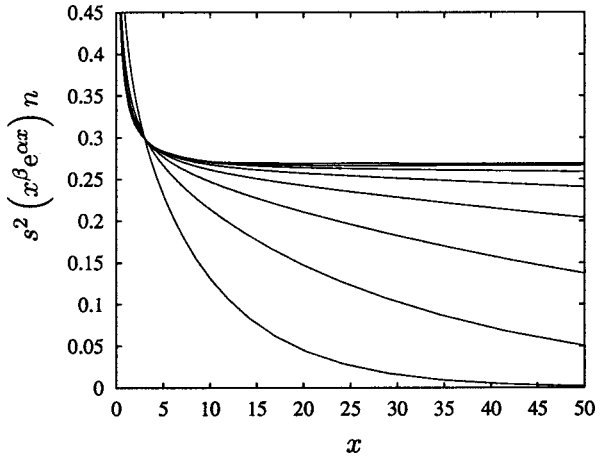

FIG. 7. Large-size tail of distribution with α, β listed below (3.10), noninteracting drops. In sequence from bottom to top of figure, profiles correspond $s=100,10^4,10^6,10^8,10^{10},10^{12},10^{16}$.

V. THERMOCAPILLARY MIGRATION

Here we consider the size distribution in a dilute suspension of spherical drops undergoing thermocapillary migration in a uniform temperature gradient. Stokes flow conditions and purely conductive heat transport are assumed. System parameters include the viscosity parameter Λ, and a conductivity parameter $\Lambda_T=1/(1+\lambda_T)$, where λ_T is the ratio of the drop- and continuous-phase thermal conductivities.

The collision kernel for thermocapillary migration is given by Eq. (2.1) with

$$K_0(u,v)=\pi U_0 v_0^{-1/3}(u^{1/3}+v^{1/3})^2|u^{1/3}-v^{1/3}|, \quad (5.1)$$

where U_0 is the thermocapillary migration velocity of an isolated drop with volume v_0 [26]. Here, time is nondimensionalized by $(\pi U_0 v_0^{-1/3} M_1)^{-1}$.

The effects of pairwise hydrodynamic and thermal interactions are incorporated through the collision efficiency E for thermocapillary motion. As in shear flow, there exists a critical size ratio below which $E=0$ [16]. The kernel functions for linear flows and thermocapillary migration are both class II in the absence of particle interactions, and become class I in the presence of particle interactions. Moreover, both collision kernels scale with the first power of drop volume; however, Eq. (5.1) is not a homogeneous function of drop volume. Nevertheless, the same long-time scaling applies to both problems, as shown by the graphs in Figs. 11 and 12, which were constructed by replotting the values calculated by Wang and Davis [16].

VI. CONCLUSIONS

The numerical results presented herein and the scaling analysis of van Dongen and Ernst [25] indicate that hydrody-

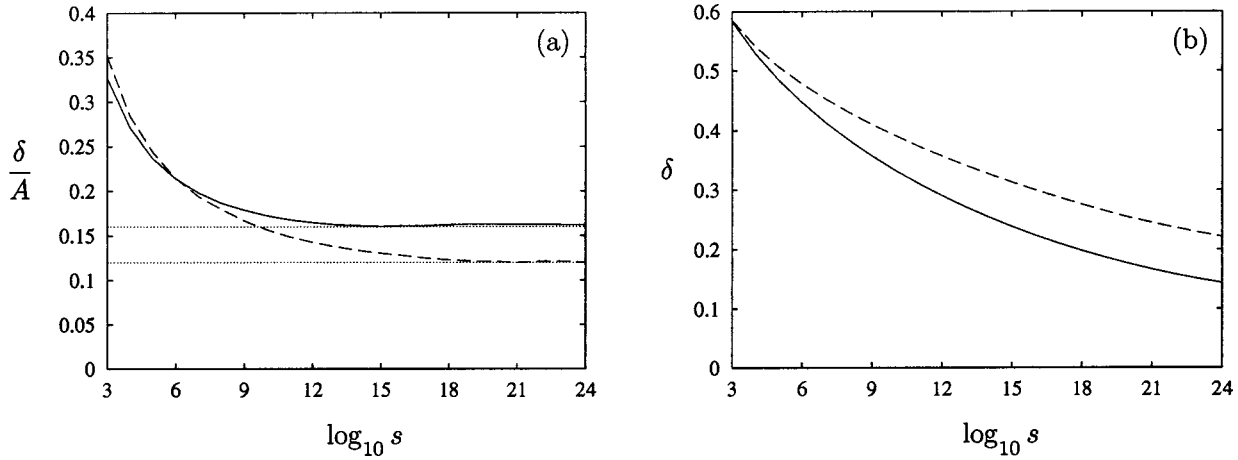

FIG. 8. Parameters for large-size tail of distribution (3.2b), $\Lambda=1/2$; shear flow (solid curves) and straining flow (dashed curves); formula (3.3) [dotted lines in (a)].

namic interactions qualitatively affect the long-time evolution of the drop size distribution in linear flows and in thermocapillary migration. According to our results, the scaling theory applies even though the kernel functions do not obey the assumed form (1.3) and (1.4), except in straining flow. However, in the presence of hydrodynamic interactions the scaling regime is attained much more slowly, particularly for the largest drops in the distribution.

Hydrodynamic interactions may have less influence on other systems. Numerical simulations show that hydrodynamic interactions do not qualitatively affect the size distribution of drops undergoing Brownian motion [16]. This is because the collision efficiency for Brownian coalescence is nonvanishing in the small size ratio limit [21]. As a result, the Brownian collision kernel is class III, whether or not hydrodynamic interactions are present.

Drop deformation was neglected in our study; this assumption is valid provided that $B \ll 1$ for all drops in the system, where $B=v^{1/3}\eta\dot{\gamma}/\sigma$ and σ is the coefficient of surface tension. For finite B, coalescence rates become sensitive to the strength of van der Waals attraction (i.e., Hamaker constant). Moreover, for a fixed value of the Hamaker constant there exists a critical drop size corresponding to $B=B^*$ beyond which coalescence is strongly hindered $E\approx 0$ [27]. Thus, a narrow drop size distribution, characterized by $B\approx B^*$ is eventually attained [17,18,22,28].

ACKNOWLEDGMENTS

We thank Dr. Alexander Zinchenko for the use of his computer subroutines to evaluate the pairwise hydrodynamic mobilities of spherical drops in linear flows. This work was supported by NASA Grant No. NAG3-2477.

APPENDIX A: COLLISION EFFICIENCIES

The relative velocity of two particles in Stokes flow is given by [29]

$$\mathbf{U}_{12}(\mathbf{r}_{12})=\frac{1}{2}\boldsymbol{\omega}\times\mathbf{r}_{12}+\mathbf{e}\cdot\mathbf{r}_{12} -[A(r_{12})\hat{\mathbf{r}}_{12}\hat{\mathbf{r}}_{12}+B(r_{12})(\hat{\mathbf{I}}-\hat{\mathbf{r}}_{12}\hat{\mathbf{r}}_{12})]\cdot\mathbf{e}\cdot\mathbf{r}_{12}, \tag{A1}$$

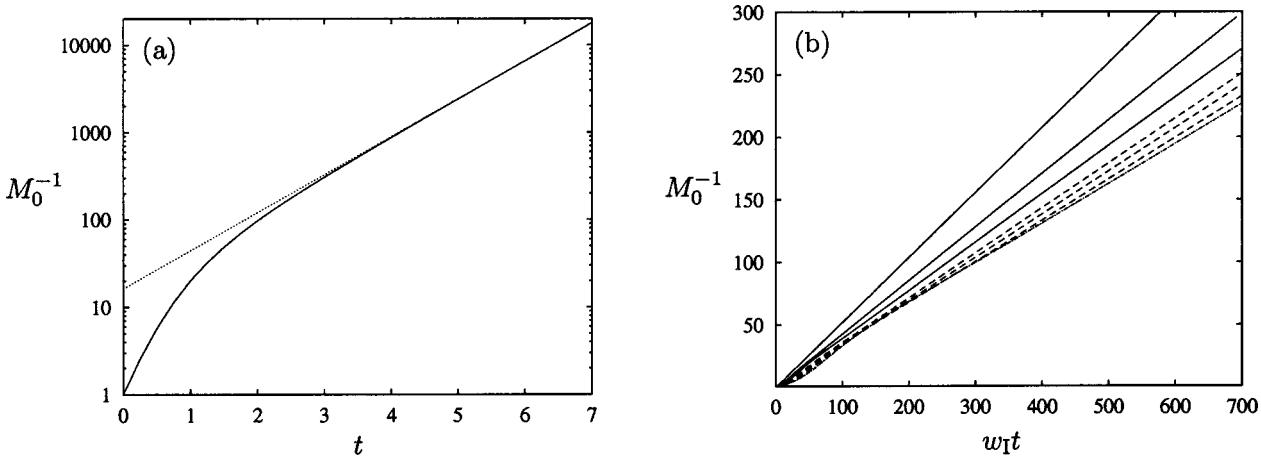

FIG. 9. Evolution of the number of drops in (a) absence, (b) presence of hydrodynamic interactions. (a) numerical result (solid curve), scaling (3.9) (dotted curve); (b) $\Lambda=1$ (dot-dashed curve); in sequence from bottom to top, profiles correspond to $\Lambda=1/2$, 1/4, $4\Lambda_0$ shear flow (solid curves), straining flow (dashed curves).

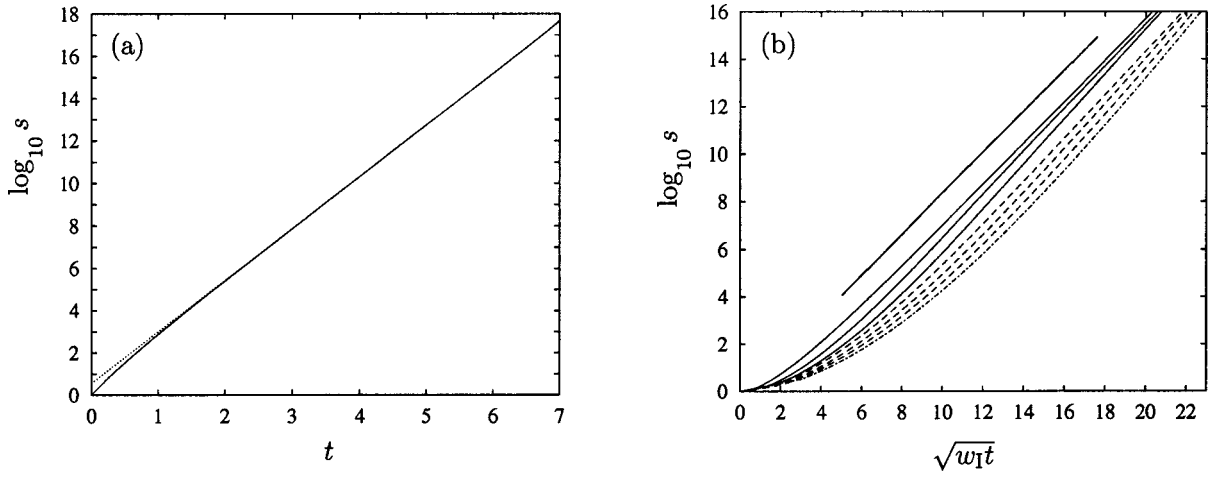

FIG. 10. Evolution of the average drop size in (a) absence, (b) presence of hydrodynamic interactions; (a) numerical result (solid curve), scaling (3.10) (dotted curve); (b) $\Lambda=1$ (dot-dashed curve); in sequence from bottom to top, profiles correspond to $\Lambda=1/2$, 1/4, $4\Lambda_0$ shear flow (solid curves), straining flow (dashed curves), scaling (3.6) (line segment).

where $\mathbf{e}$ and $\boldsymbol{\omega}$ are the rate-of-strain tensor and vorticity of the ambient linear flow field respectively, $\hat{\mathbf{I}}$ is the identity tensor, $\mathbf{r}_{12}$ is the relative position of the drop centers, $r_{12}=|\mathbf{r}_{12}|$ is the center-to-center separation, and $\hat{\mathbf{r}}_{12}=\mathbf{r}_{12}/r_{12}$ is the unit orientation vector. Pairwise hydrodynamic interactions enter through the scalar pair mobility functions A and B which depend on the size ratio of the drops κ the viscosity ratio λ, and the center-to-center separation r_{12}.

Equation (A1) can be integrated [23] to yield pair collision efficiencies for drops in axisymmetric straining flow:

$$E_{st}=e^{-3I_{st}(r_{12}^*)}, \tag{A2}$$

and in simple shear flow:

$$E_{sh}=[E_{st}^{2/3}-I_{sh}(r_{12}^*)]^{3/2}, \quad E_{st}^{2/3}\geqslant I_{sh}(r_{12}^*), \tag{A3}$$

$$E_{sh}=0, \quad E_{st}^{2/3}\leqslant I_{sh}(r_{12}^*). \tag{A4}$$

Here, I_{st} and I_{sh} are the mobility function integrals

$$I_{st}(r_{12})=\int_{r_{12}}^{\infty}\frac{A(t)-B(t)}{1-A(t)}\frac{dt}{t}, \tag{A5}$$

and

$$I_{sh}(r_{12})=\int_{r_{12}}^{\infty}\frac{tB(t)}{1-A(t)}e^{-2I_{st}(t)}\,dt. \tag{A6}$$

The collision surface is defined by $r_{12}=r_{12}^*$, where r_{12}^* is the sum of the two drop radii.

Collision efficiencies were evaluated by numerical integration of Eq. (A5) and (A6) with mobility functions A and B obtained from a solution of the Stokes equations in bispherical coordinates [20].

Calculated collision efficiencies for straining flow E_{st} and shear flow E_{sh} are shown in Fig. 13. Collision efficiencies depend on the size ratio, viscosity ratio, and flow type; by

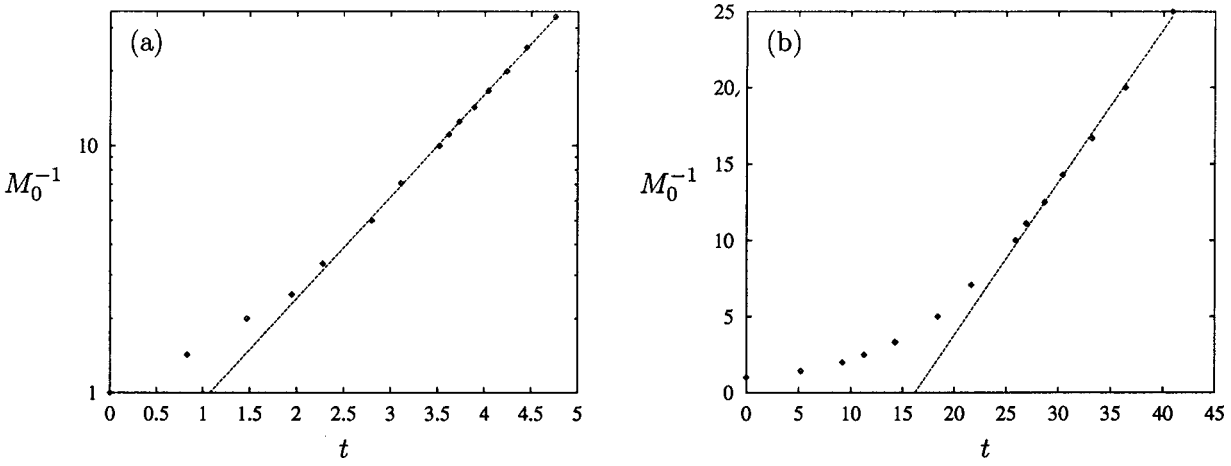

FIG. 11. Evolution of the number of drops in thermocapillary migration in (a) absence, (b) presence of hydrodynamic interactions; numerical results from Ref. [16] (symbols); scaling (3.5), and (3.9) (dotted curves); $\Lambda=\Lambda_T=1/3$; Gaussian initial size distribution, unit mean volume, standard deviation 0.2.

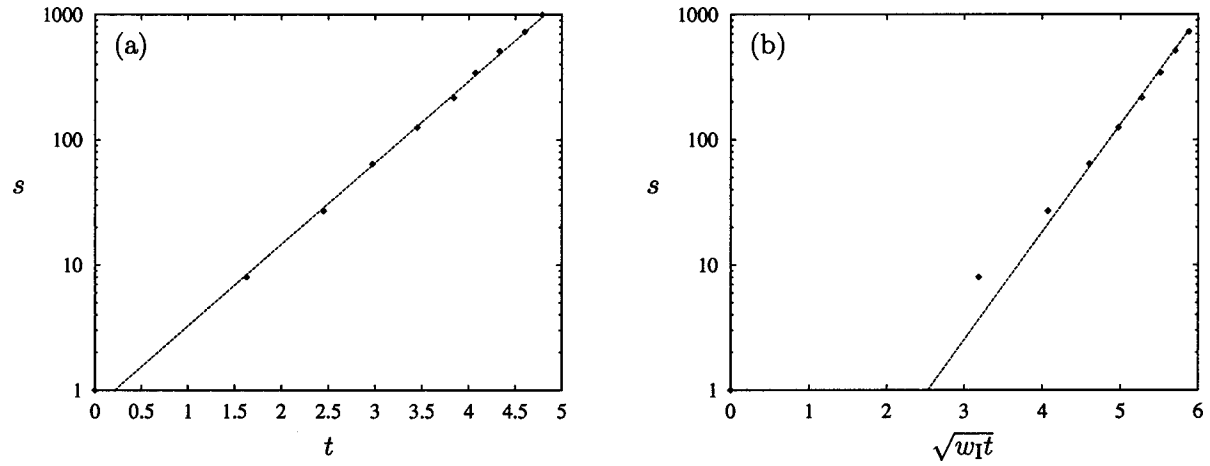

FIG. 12. Evolution of the average drop size in thermocapillary migration in (a) absence, (b) presence of hydrodynamic interactions; numerical results from Ref. [16] (symbols); scaling (3.6) and (3.10) with $w_I=1$, $w_{II}=1.5$ (dotted curve); system parameters as in Fig. 11.

symmetry $E(\kappa,\lambda)=E(\kappa^{-1},\lambda)$. As a consequence of hydrodynamic interactions, $E<1$. The results show that collision efficiencies decrease for extreme size ratios and large viscosity ratios. In the absence of hydrodynamic interactions, $A=B=0$, we recover $E=1$ according to Eqs. (A2)–(A6). The transverse mobility B vanishes for $\lambda=0$ but is otherwise positive, and the quantity $1-A$ is always positive. It follows that

$$E_{sh}\leqslant E_{st}, \tag{A7}$$

according to Eqs. (A3) and (A6). The equality holds for $\lambda=0$.

For small size ratios, an estimate for the collision efficiency in straining flow is obtained by approximating the trajectories of much smaller drops with the streamlines of the undisturbed flow field around a larger drop. Under the assumption that coalescence occurs for trajectories that intercept the collision surface, we obtain

$$E_{st}\sim\kappa^{1/3}, \quad \kappa\ll 1, \tag{A8}$$

consistent with the results shown in Fig. 13(a).

In shear flow, the collision surface is completely enclosed by a region of finite trajectories for size ratios smaller than a critical value κ_0 [23] which satisfies

$$e^{-3I_{st}(r_{12}^*)}-I_{sh}(r_{12}^*)=0, \tag{A9}$$

according to Eqs. (A2) and (A3). The collision efficiency vanishes as

$$E_{sh}\sim(\kappa-\kappa_0)^{3/2} \tag{A10}$$

for $\kappa\to\kappa_0$. For $\kappa<\kappa_0$, $E_{sh}=0$. The critical size ratio increases with λ, as seen in Fig. 13(b). Solving Eq. (A9) numerically, we find

$$\kappa_0=1 \text{ for } \Lambda<\Lambda_0, \tag{A11}$$

where

$$\Lambda_0\simeq 7.727\times 10^{-3}. \tag{A12}$$

For $\Lambda<\Lambda_0$, all drop size distributions are stationary in shear flow.

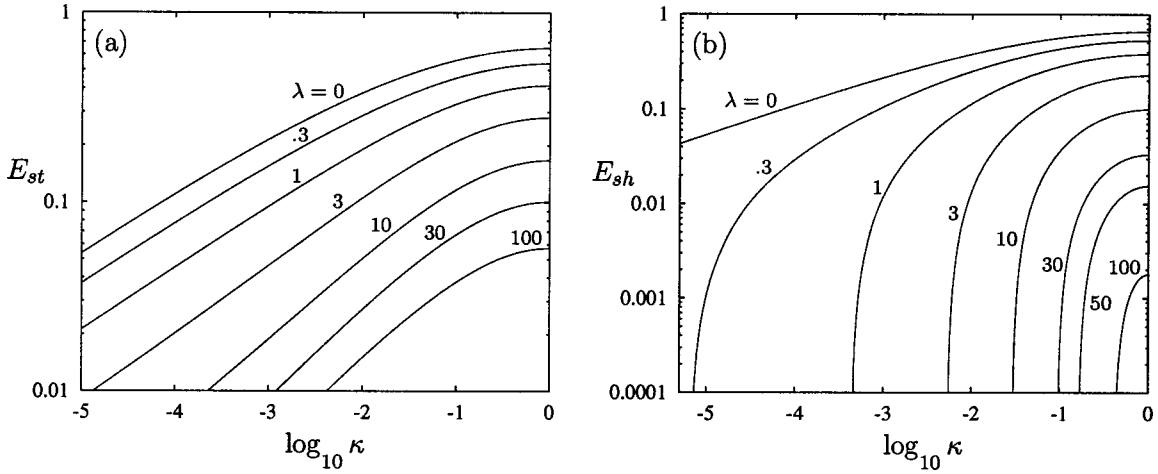

FIG. 13. Collision efficiencies for straining flow (a), shear flow (b); viscosity ratio λ as indicated.

[1] D. Rosenfeld, Y. Rudich, and R. Lahav, Proc. Natl. Acad. Sci. U.S.A. **98**, 5975 (2001).
[2] U. Sundararaj and C.W. Macosko, Macromolecules **28**, 647 (1995).
[3] D.E. Rosner, R. McGraw, and P. Tandon, Ind. Eng. Chem. Res. **42**, 699 (2003).
[4] J. Senee, B. Robillard, and M. Vignes-Adler, Food Hydrocolloids **13**, 15 (1999).
[5] J.A. Remirez, A. Zinchenko, M. Loewenberg, and R.H. Davis, Chem. Eng. Sci. **54**, 149 (1999).
[6] M. Smoluchowski, Z. Phys. Chem. (Munich) **92**, 129 (1917).
[7] D. Ramkrishna, *Population Balances: Theory and Applications to Particulate Systems in Engineering* (Academic, New York, 2000).
[8] P.G.J. van Dongen and M.H. Ernst, Phys. Rev. Lett. **54**, 1396 (1985).
[9] S.K. Friedlander and C.S. Wang, J. Colloid Interface Sci. **22**, 126 (1966).
[10] C.S. Wang and S.K. Friedlander, J. Colloid Interface Sci. **24**, 170 (1967).
[11] James R. Hunt, J. Fluid Mech. **122**, 169 (1982).
[12] Paul Meakin, Tamás Vicsek, and Fereydoon Family, Phys. Rev. B **31**, 564 (1985).
[13] J.R. Rogers and R.H. Davis, Metall. Trans. A **21**, 59 (1990).
[14] C. Oh and C.M. Sorensen, J. Aerosol Sci. **28**(6), 937 (1997).
[15] Jan R. Rogers and Robert H. Davis, J. Atmos. Sci. **47**, 1075 (1990).
[16] Hua Wang and Robert H. Davis, J. Colloid Interface Sci. **159**, 108 (1993).
[17] Michael A. Rother and Robert H. Davis, J. Colloid Interface Sci. **214**, 297 (1999).
[18] Michael A. Rother and Robert H. Davis, Phys. Fluids **13**, 1178 (2001).
[19] D.L. Wright, R. McGraw, and D.E. Rosner J. Colloid Interface Sci. **236**, 242 (2001).
[20] H. Wang, A.Z. Zinchenko, and R.H. Davis, J. Fluid Mech. **265**, 161 (1994).
[21] X. Zhang and R.H. Davis, J. Fluid Mech. **230**, 479 (1991).
[22] B.E. Burkhart, P.V. Gopalkrishnan, S. Hudson, A.M. Jamieson, M.A. Rother, and R.H. Davis, Phys. Rev. Lett. **87**, 098304 (2001).
[23] A.Z. Zinchenko, Prikl. Mat. Mekh. **47**, 56 (1984).
[24] R.H. Davis, J.A. Schonberg, and J.M. Rallison, Phys. Fluids **145**, 179 (1984).
[25] P.G.J. van Dongen and M.H. Ernst, J. Stat. Phys. **50**, 295 (1988).
[26] M.J. Block N.O. Young, and J.S. Goldstein, J. Fluid Mech. **6**, 350 (1959).
[27] M. B. Nemer, X. Chen, D. H. Papadopoulos, J. Blawzdziewicz, and M. Loewenberg (unpublished).
[28] A. Nandi, A. Mehra, and D.V. Khakhar, Phys. Rev. Lett. **83**, 2461 (1999).
[29] G.K. Batchelor and J.T. Green, J. Fluid Mech. **56**, 375 (1972).